In their response to electric fields, secretory granule matrices behave like smart synthetic polymers, which have been used as drug carriers, sensors, valves, engines, and actuators (*20*). However, the speed, size, and electrical properties of granule matrices distinguish them from other gels and make them ideal for use in the design of fast chemoelectromechanical devices.

REFERENCES AND NOTES

1. J. M. Fernandez, M. Villalon, P. Verdugo, *Biophys. J.* **59**, 1022 (1991).
2. M. J. Curran and M. S. Brodwick, *J. Gen. Physiol.* **98**, 771 (1991).
3. Isolated secretory granules were prepared by sonification of purified beige (bg^J/bg^J) mouse mast cells that were obtained by peritoneal lavage (*21*). Some of these granules were devoid of membranes, and others lost their membranes within a few hours after exposure to the bathing solution. Granule matrices that were devoid of an intact granular membrane were recondensed by exposure to an acidic solution that contained histamine (*1, 2*). A condensed matrix was inserted into the tip of a glass pipette with the application of suction. The pipette voltage relative to the bath was controlled by a current-to-voltage converter. In one case, we cut a piece of a swollen matrix; this piece had the same electrical properties of a whole matrix, which indicates that the properties of the matrix do not depend on remnants of the granule membrane. Furthermore, granule matrices that were pretreated with Triton-X (30% in histamine saline) gave similar results. Glass pipettes had tip resistances of 5 to 15 megohms in the histamine solution. Unless otherwise specified, the solution in both the bath and the pipette contained 12 mM histamine dichloride and 0.5 mM citric acid (pH 3.5). The current-to-voltage converter had a gain of 1.2 mV nA^{-1} and was followed by a unity-gain differential amplifier. We used an IDA interface (INDEC Systems, Sunnyvale, CA) with a COMPAQ 386-25 computer and the CCLAMP software (INDEC Systems) to apply the voltages and to sample the currents at 2.5-ms intervals. To measure the swelling, we imaged isolated granule matrices and analyzed them as described (*1, 21*).
4. We observed similar voltage-dependent behavior in all 36 granule matrices. In all cases, the time course of the current was very similar (compare Figs. 1B, 2A, and 3A). In two cases we did a frame-by-frame analysis (~45 frames per experiment) of swelling in response to a voltage pulse. The time courses were similar with an instantaneous phase (≤30 ms) and a slower phase with a time constant of 212 ms for one matrix at −2.5 V (Fig. 1) and 422 ms for the second matrix at −1.8 V. Relative swelling was calculated as A_t/A_0, where A_t is the cross-sectional area at an arbitrary time t and A_0 is the cross-sectional area 165 ms before the onset of the voltage. The data correspond to the swelling of a single granule matrix in response to a single voltage pulse. Cross-sectional areas for each frame were measured seven times, and each data point represents the mean ± SD.
5. E. H. Nielsen, *J. Cell Sci.* **96**, 43 (1990).
6. To measure the force exerted by a swollen granule, we brought a condensed granule close to a stress-transducing beam (SensoNor, Horten, Norway), which consists of two active resistors whose resistance changes as the beam is bent. These resistors form two legs of a Wheatstone bridge, and two passive resistors make up the remaining two legs. The output voltage from the bridge was filtered (band-pass filter, corner frequencies 0 and 3 Hz), amplified (×10^5), and sampled by the computer at 6.36-ms intervals. We calibrated the transducer by placing a weight at its edge and measuring the resulting voltage.
7. In several instances, the force exerted when the granule was subjected to the first voltage pulse was larger than the force exerted on subsequent pulses because the granule was pushed up and cut by the glass pipette.
8. When the granule was pushed out, we observed an abrupt decrease in current to a level that corresponded to the current through the pipette alone. These changes were reversed when the granule was brought back into the glass pipette with suction and formed a tighter electrical seal.
9. The matrix conductance changed from 4.6 ± 5 nS (range, 0.72 to 15 nS; n = 8) at positive potentials to 480 ± 40 nS (range, 440 to 560 nS; n = 8) at negative potentials. The relative conductance was, however, underestimated because we did not correct for the leak current through the pipette-matrix seal. This leak current could account for most of the current at positive voltages.
10. The pipette conductance was 130 ± 50 nS (range, 70 to 200 nS; n = 5). At negative potentials, the matrix current exceeded the pipette current by a factor of 4.21 ± 1.55 (range, 2.50 to 6.14; n = 5).
11. The mean instantaneous and steady-state conductances at negative voltages were 352 ± 48 nS (range, 280 to 400 nS; n = 4) and 470 ± 35 nS (range, 430 to 510 nS; n = 4), respectively.
12. A. R. Blythe, *Electrical Properties of Polymers* (Cambridge Univ. Press, Cambridge, 1979).
13. T. Tanaka, *Sci. Am.* **244**, 124 (January 1981); ———, I. Nishio, S.-T. Sun, S. Ueno-Nishio, *Science* **218**, 467 (1982).
14. T. Tanaka and D. J. Fillmore, *J. Chem. Phys.* **70**, 1214 (1979).
15. J. M. Fernandez, E. Neher, B. D. Gomperts, *Nature* **312**, 453 (1984).
16. W. Almers, *Annu. Rev. Physiol.* **52**, 607 (1990); C. Nanavati, V. S. Markin, A. F. Oberhauser, J. M. Fernandez, *Biophys. J.* **63**, 1118 (1992).
17. L. J. Breckenridge and W. Almers, *Proc. Natl. Acad. Sci. U.S.A.* **84**, 1945 (1987).
18. ———, *Nature* **328**, 814 (1987).
19. P. Y. Tam and P. Verdugo, *ibid.* **292**, 340 (1981).
20. I. C. Kwon, Y. H. Bae, S. W. Kim, *ibid.* **354**, 291 (1991); Y. Osada, H. Okuzaki, H. Hori, *ibid.* **355**, 242 (1992); K. Kajiwara and S. B. Ross-Murphy, *ibid.*, p. 208; D. DeRossi, Y. Osada, A. Yamauchi, *Polymer Gels: Fundamentals and Biomedical Applications* (Plenum, New York, 1991); I. Z. Steinberg, A. Oplatka, A. Katchalsky, *Nature* **210**, 568 (1966).
21. J. R. Monck, A. F. Oberhauser, G. Alvarez de Toledo, J. M. Fernandez, *Biophys. J.* **59**, 39 (1991).
22. Relative swelling is calculated as A_V/A_0, where A_V and A_0 are the cross-sectional areas at an arbitrary voltage and at 0 V, respectively. Each point is the mean ± SD for five measurements of cross-sectional area made on the same image. We used a long depth-of-field objective for three of eight experiments. For these three experiments, the swelling had a slope that was 0.35 to 0.77 relative-swelling unit per volt. For the remaining five experiments, we used a short depth-of-field objective. The swelling had a slope of 0.061 to 0.18 relative-swelling unit per volt. On swelling, the matrix was probably going out of the plane of focus of the shorter depth objective, which would result in an apparently smaller relative swelling. The experiment shown in Fig. 2C was conducted with a short depth-of-field objective.

23. We thank P. Verdugo, J. L. Rae, and M. McNiven for comments.

19 October 1992; accepted 23 December 1992

Structure of the Thiamine- and Flavin-Dependent Enzyme Pyruvate Oxidase

Yves A. Muller and Georg E. Schulz*

Pyruvate oxidase from *Lactobacillus plantarum* is a tetrameric enzyme that decarboxylates pyruvate, producing hydrogen peroxide and the energy-storage metabolite acetylphosphate. Structure determination at 2.1 angstroms showed that the cofactors thiamine pyrophosphate (TPP) and flavin adenine dinucleotide (FAD) are bound at the carboxyl termini of six-stranded parallel β sheets. The pyrophosphate moiety of TPP is bound to a metal ion and to a βααβ unit corresponding to an established sequence fingerprint. The spatial arrangement of TPP and FAD suggests that the oxidation of the oxyethyl intermediate does not occur by hydride displacement but rather by a two-step transfer of two electrons.

Pyruvate oxidase (E.C. 1.2.3.3) is important in the aerobic growth of lactobacteria (*1*). The enzyme (E) catalyzes the oxidative decarboxylation of pyruvate in several steps

$$\text{Pyruvate} + \text{TPP-E-FAD}_{ox} \rightleftharpoons \text{Oxyethyl-TPP-E-FAD}_{ox} + CO_2 \quad (1)$$

$$\text{Oxyethyl-TPP-E-FAD}_{ox} \rightleftharpoons \text{Acetyl-TPP-E-FAD}_{red} \quad (2)$$

$$\text{Acetyl-TPP-E-FAD}_{red} + O_2 \rightleftharpoons \text{Acetyl-TPP-E-FAD}_{ox} + H_2O_2 \quad (3)$$

Institut für Organische Chemie und Biochemie, Albert-Ludwigs-Universität, W-7800 Freiburg im Breisgau, Germany.

*To whom correspondence should be addressed.

$$\text{Acetyl-TPP-E-FAD}_{ox} + P_i \rightleftharpoons \text{Acetylphosphate} + \text{TPP-E-FAD}_{ox} \quad (4)$$

where P_i is inorganic phosphate. The released energy is partially stored in acetylphosphate, which can be used by acetate kinase to convert adenosine diphosphate to adenosine triphosphate (*1*). The enzyme requires TPP, FAD, and a divalent cation such as Mn^{2+} for catalytic activity. Sequence similarity in the TPP binding region suggests that pyruvate oxidase is related to the important enzyme pyruvate decarboxylase (*2*), which, however, does not oxidize the substrate and thus lacks FAD.

Recombinant pyruvate oxidase from

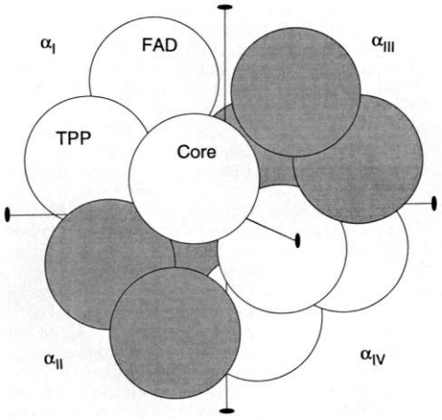

Fig. 1. Schematic drawing of the homotetrameric enzyme pyruvate oxidase. The D_2 point group symmetry of the α_4 molecule is indicated by the twofold axes. Each circle represents a domain. Subunits are indicated by shading. The active sites are located at the interfaces α_I-α_{II} and α_{III}-α_{IV}, which are larger than the interfaces α_I-α_{III} and α_{II}-α_{IV}. The crystallographic asymmetric unit contains dimer α_I-α_{III}.

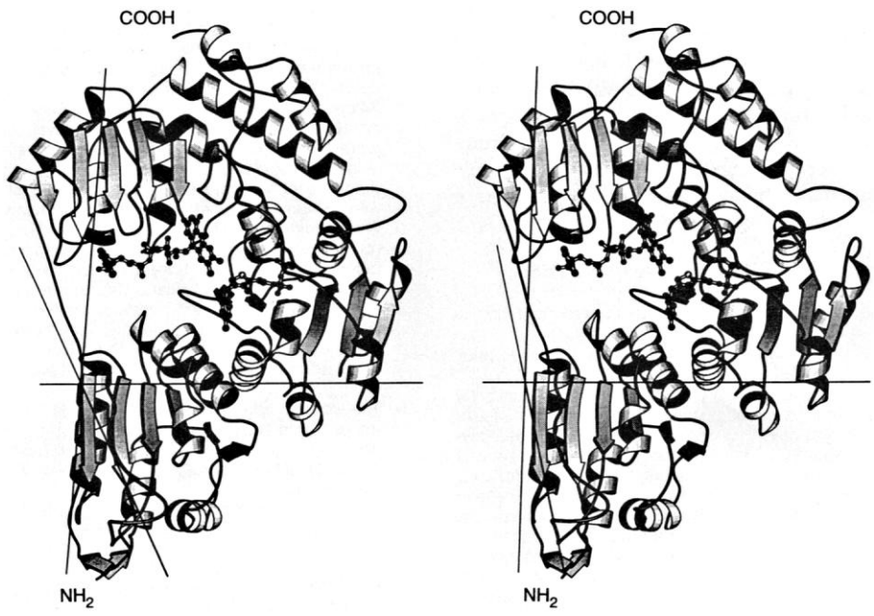

Fig. 2. Stereo view representation of pyruvate oxidase prepared with the program MOLSCRIPT (*23*) showing secondary structure and cofactors.

Lactobacillus plantarum has been engineered for improved stability by three point mutations (*3*, *4*). Enzyme crystals belonged to space group $C222_1$ (cell dimensions, a = 122 Å; b = 155 Å; c = 167 Å) and contained two subunits in the crystallographic asymmetric unit (*5*). The refined model consisted of a dimer with 9048 nonhydrogen polypeptide atoms, 2 TPP and 2 FAD molecules, 2 Mg^{2+} ions, and 748 water molecules. The crystallographic R factor was 16.3% for all data between 10 and 2.1 Å. The root-mean-square deviations from ideal bond lengths and angles were 0.014 Å and 2.7°, respectively.

Pyruvate oxidase is a homotetramer with symmetry D_2 (Fig. 1). The monomer is divided into three domains, each of which contains a six-stranded parallel β sheet surrounded by α helices (Fig. 2). The first domain (core domain, residues 9 to 191) forms the core of the tetramer. It is linked by a chain segment lacking secondary structure to the FAD-binding domain (FAD domain, residues 192 to 342). The third domain binds TPP (TPP domain, residues 343 to 593). In our assignment, the third domain includes a long α helix connecting it to the FAD domain as well as a 50-residue extension at the COOH-terminus (6). The four core domains are closely packed at the intersection of the three molecular twofold axes at the tetramer center; the remaining free space is as small as about 100 $Å^3$.

Cofactor FAD binds at the β strand ends of the parallel six-stranded β sheet of the FAD domain. This sheet has the topology of a twofold Rossmann fold (*7*) in which, however, only two of the five connections between β strands contain α helices (Fig. 3). In contrast to the usual binding mode of nicotinamide adenine dinucleotide to a Rossmann fold, the adenosine moiety of FAD is attached to the second βαβαβ unit instead of the first one. There is no Gly sequence fingerprint for dinucleotide binding and no βαβ unit for binding pyrophosphate (8, 9); rather, the phosphate groups of FAD are hydrogen-bonded to NH groups of extended peptide chain segments after the first and fourth strand of the β sheet and to His^{101} from the core domain. In common with other dinucleotide proteins (*10*), pyruvate oxidase binds the hydroxyl groups of the adenosine ribose of FAD with an acidic residue at the end of the second strand of the respective βαβαβ unit (Asp^{306} on fifth strand of the sheet). The isoalloxazine ring of FAD is surrounded by a shell of six aromatic residues (three phenylalanine and three tyrosine residues) and is bent along the N-10 . . . N-5 axis (a dihedral angle of 15°). This constraint favors the reduced form of FAD and thus increases its redox potential.

The topology of the six-stranded β sheet to which TPP is bound (Fig. 3) is identical to that of the core domain but differs from the topologies of nucleotide-binding proteins (9). As observed for TPP binding in transketolase (*11*), pyruvate oxidase binds the pyrophosphate group of TPP with a metal ion (*12*, *13*) and with the

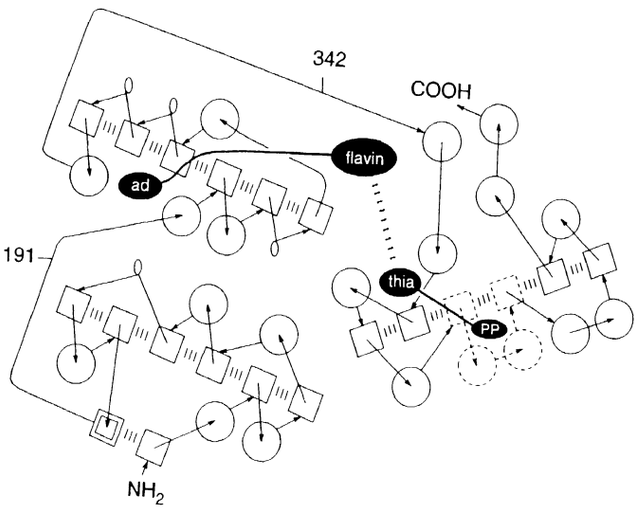

Fig. 3. Sketch of the chain fold and cofactor binding sites from approximately the same view as in Fig. 2. The cofactors (black) as well as the three domains (NH_2-terminal core domain, FAD-binding domain, and TPP-binding domain) and the sequence fingerprint indicative of TPP binding (*14*) (broken lines) are emphasized. Two electrons are transferred from TPP to FAD (Eq. 2). β Strands (squares and concentric squares), hydrogen bonds within β sheets (III), and α helices (circles) are as shown.

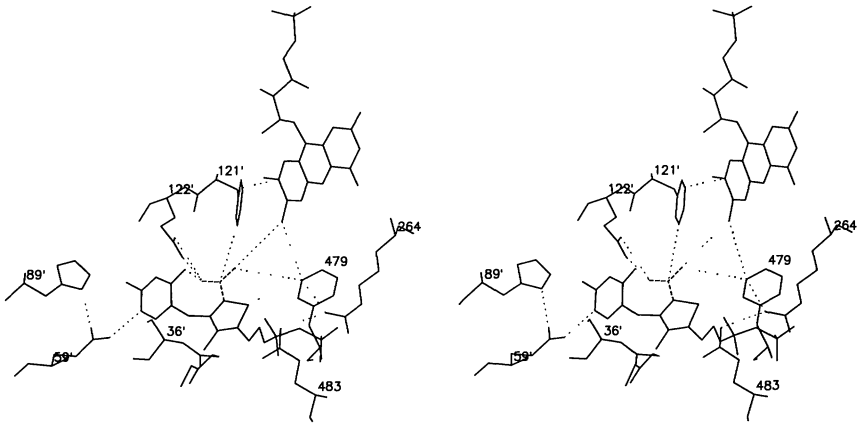

Fig. 4. Stereo view of the active center, including TPP and the flavin mononucleotide moiety of FAD. Hypothetical planar oxyethyl anion bound to C-2 of TPP (broken lines). Distances (*24*) important for stabilization and electron transfer (dotted lines) are shown. Only the residues suggested to be important for catalysis are displayed ($Gly^{35'}$, $Ser^{36'}$, $Glu^{59'}$, $His^{89'}$, $Phe^{121'}$, $Gln^{122'}$, Arg^{264}, Phe^{479}, and Glu^{483}).

fingerprint sequence X_5-Gly-Asp-Gly-Y_{25-28}-Asn (*14*) that forms a βααβ unit (Fig. 3). The metal ion is bound in octahedral arrangement to an oxygen molecule from each phosphate group, to Asp^{447}-OD1 (fingerprint), Asn^{474}-OD1 (fingerprint), Gln^{476}-O, and to a water molecule. Gly^{448} (fingerprint) and Gly^{449} are in the first turn of an α helix and bind a phosphate group, as has been observed in several dinucleotide-binding proteins. Because the sequence fingerprint has been found in various proteins (*14*), this βααβ motif for TPP binding is rather general.

The TPP conformation is similar to the observed conformation in transketolase, juxtaposing the 4′α-NH_2 group of the pyrimidine with the reactive C-2 of the thiazole ring (Fig. 4). Moreover, there is a carboxylate ($Glu^{59'}$ of the neighboring subunit) that hydrogen bonds to N-1′ of the pyrimidine ring, which could tautomerize to produce a 4′α-imino group (*15*). This imino group could function as a base picking up the acid proton at C-2 of the thiazole ring (*16*) because the N-4′α . . . C-2 distance is 3.2 Å with a favorable geometry. There is no other base around C-2. The environment of the thiazole ring is mostly nonpolar.

The activated C-2 attacks pyruvate, giving rise to decarboxylation (Eq. 1). In view of the observed structure, we suggest that subsequent oxidation of the oxyethyl-TPP intermediate by cofactor FAD (Eq. 2) does not occur by hydride displacement (*16*) from C-2α of oxyethyl-TPP (previously the carbonyl carbon of pyruvate) to N-5 of the isoalloxazine of FAD. There is no acidic group available to protonate C-2α, and the hydride ion would have to traverse 9.5 Å without a relay station. More likely, oxidation occurs by a two-step transfer of two electrons to the isoalloxazine ring, probably relayed by the benzene ring of Phe^{479} or $Phe^{121'}$ (or both) (Fig. 4). An additional electron in Phe^{479} could be stabilized by close contact to the guanidinium group of Arg^{264}, which is restrained by Glu^{483} (Fig. 4).

The reduced FAD would then donate its electrons to the final electron acceptor, O_2, by forming an isoalloxazine C-4a-hydroperoxide intermediate as described for *p*-hydroxybenzoate hydroxylase (*17*) and releasing H_2O_2 (Eq. 3). C-4a is accessible to O_2 from the solvent. Finally, TPP would be regenerated by attack of P_i, liberating acetylphosphate (Eq. 4). A binding site for the P_i would be provided by the peptide amides of residues 35′ and 36′ from the other subunit. We have assumed that there is no major conformational change during catalysis, consistent with the observation that the crystals withstand high concentrations of pyruvate (*18*).

REFERENCES AND NOTES

1. F. Goetz and B. Sedewitz, in *Biochemistry and Physiology of Thiamin Diphosphate Enzymes*, H. Bisswanger and J. Ullrich, Eds. (Verlag Chemie, Weinheim, Germany, 1991), pp. 286–293; G. Schumacher *et al.*, in *ibid.*, pp. 300–307.
2. J. B. Green, *FEBS Lett.* **246**, 1 (1989).
3. Large amounts of the enzyme were provided by Boehringer-Mannheim GmbH (Penzberg, Germany).
4. B. Risse, G. Stempfer, R. Rudolph, H. Möllering, R. Jaenicke, *Protein Sci.*, in press; B. Risse, G. Stempfer, R. Rudolph, G. Schumacher, R. Jaenicke, *ibid.*, in press.
5. Enzyme crystals were grown according to the hanging drop method. A 20-μl drop of a solution containing enzyme (20 mg/ml) in 50 mM potassium phosphate buffer (pH 5.2), 5% (v/v) glycerol, 0.5 M ammonium sulfate, and 1 mM TPP was placed over a reservoir containing the same buffer, 10% (v/v) glycerol, and 0.95 M ammonium sulfate. Crystals growing to ~80 × 100 × 500 μm^3 were obtained within 3 months. The structure was solved by the multiple isomorphous replacement method with the use of non-crystallographic symmetry (NCS). Native and heavy atom derivative data were collected to 3 Å resolution on a multiwire area detector (model X1000, Siemens/Nicolet) at 4°C with a rotating anode x-ray source (model RU200B, Rigaku). In addition, a native data set to 2.1 Å resolution with an overall completeness of 96% and an internal R_{sym} value of 12.2% was obtained with synchrotron radiation (wavelength, 1.01 Å) with the use of an image plate at the EMBL outstation at Deutsches Elektronensynchrotron (DESY) (Hamburg, Germany). An electron density map calculated from seven derivatives at 3.0 Å resolution did not allow complete chain tracing but yielded the outline of the subunits. The subunit relations were established with the program POLARRFN (*19*) in the resolution range 8.0 to 5.0 Å, which showed point group symmetry D_2 for the homotetramer. Subsequent NCS density averaging (*20*) at 3.5 Å resolution resulted in a map that was interpretable for residues 9 to 593 of each polypeptide (*6*) and for the cofactors TPP and FAD. Program-O was used to build the model into the density (*21*). The model was then refined with XPLOR (*22*). In the last two rounds of the refinement, the NCS restraints were completely removed.
6. Each subunit contains 603 residues (*4*). The first eight and last ten residues of the chain could not be located in the crystal.
7. S. T. Rao and M. G. Rossmann, *J. Mol. Biol.* **76**, 241 (1973).
8. R. K. Wierenga, M. C. H. De Maeyer, W. G. J. Hol, *Biochemistry* **24**, 1346 (1985).
9. G. E. Schulz, *Curr. Opin. Struct. Biol.* **2**, 61 (1992).
10. P. A. Karplus and G. E. Schulz, *J. Mol. Biol.* **195**, 701 (1987).
11. Y. Lindqvist, G. Schneider, U. Ermler, M. Sundström, *EMBO J.* **11**, 2373 (1992); M. Sundström, Y. Lindqvist, G. Schneider, *FEBS Lett.* **313**, 229 (1992).
12. R. Blake, T. A. O'Brien, R. B. Gennis, L. P. Hager, *J. Biol. Chem.* **257**, 9605 (1982).
13. The metal ion is here modeled as Mg^{2+}. The density is sufficient for Ca^{2+} but not for Mn^{2+}
14. C. F. Hawkins, A. Borges, R. N. Perham, *FEBS Lett.* **255**, 77 (1989).
15. A. Schellenberger, *Chem. Ber.* **123**, 1489 (1990).
16. D. J. Rawn, *Biochemistry* (Harper & Row, New York, 1983), pp. 414–417.
17. H. Schreuder, W. G. H. Hol, J. Drenth, *Biochemistry* **29**, 3101 (1990).
18. As determined in a separate experiment by soaking the crystals in the hanging drop reservoir solution with 10 mM pyruvate for several days.
19. Collaborative Computing Project 4, Daresbury Laboratory, Warrington, United Kingdom (1979).
20. G. Bricogne, *Acta Crystallogr.* **32**, 832 (1976).
21. T. A. Jones, J.-Y. Zou, S. W. Cowan, M. Kjeldgaard, *ibid.* **47**, 110 (1991).
22. A. T. Brunger, J. Kuriyan, M. Karplus, *Science* **235**, 458 (1987).
23. P. Kraulis, *J. Appl. Crystallogr.* **24**, 946 (1991).
24. The distances shown are as follows: $His^{89'}$-ND1 . . . $Glu^{59'}$-OE1 = 2.8 Å; $Glu^{59'}$-OE2 . . . N-1′ (TPP) = 2.6 Å; N-4′α(TPP) . . . Oβ(TPP) = 2.3 Å; $Gln^{122'}$-OE1 . . . Oβ(TPP) = 3.4 Å; $Gln^{122'}$-NE2 . . . Oβ(TPP) = 3.4 Å; C-2α(TPP) . . . $Phe^{121'}$-CE2 = 5.4 Å; $Phe^{121'}$-CE1 . . . C-8(FAD) = 3.7 Å; C-2β(TPP) . . . Phe^{479}-CE2 = 4.5 Å; Phe^{479}-CE2 . . . C-7α(FAD) = 4.1 Å; C-2β(TPP) . . . C-7α(FAD) = 4.2 Å; Phe^{479}-CE2 . . . Arg^{264}-NH1 = 3.4 Å; and Arg^{264}-NH1 . . . Glu^{483}-OE2 = 3.0 Å. C-2α(TPP), C-2β(TPP), and Oβ(TPP) are, respectively, the former carbonyl carbon, methyl carbon, and carbonyl oxygen of pyruvate.

25. We thank the Boehringer-Mannheim GmbH (Penzberg, Germany) for support; R. Rudolph and H. Möllering for discussions; and the team of the EMBL outstation at DESY (Hamburg) for help in collecting native data. The coordinates are deposited with the Protein Data Bank, Brookhaven, N.Y.

27 October 1992; accepted 14 January 1993